Chap. 9 : Temperature phase transitions in $Rb_2KRe_3^{+}F_6$ elpasolites

Raman spectroscopy study

A. Vtyurin (1,2), A. Krylov (1), S. Krylova (1), Yu. Gerasimova (1,2), A. Ivanenko (1), V. Voronov (1)

(1) Kirensky Institute of Physics, Federal Research center KSC SB RAS, Krasnoyarsk, Russia
(2) Siberian Federal University, Krasnoyarsk, Russia

Corresponding author: vtyurin@iph.krasn.ru

Abstract: Phase transitions in crystals of fluorine-containing elpasolites are investigated by Raman scattering spectroscopy. It was found that lattice instabilities in these crystals are induced by soft mode condensations, while restorations of these modes in the distorted phases have not been observed due to their strong interactions with low-frequency noncritical lattice vibrations. Increasing the mass of a rare-earth ions shifts down frequencies of noncritical modes, that enhances these interactions and leads to a narrowing of the range of existence of intermediate phase and then to its disappearance.

Keywords: ELPASOLITES, RAMAN SPECTROSCOPY, PHASE TRANSITIONS, SOFT MODES, HARD MODES

Cite this paper: A. Vtyurin, A. Krylov, S. Krylova, Yu. Gerasimova, A. Ivanenko, V. Voronov, OAJ materials and Devices, vol 5(1) – chap No9 in "Perovskites and other Framework Structure Crystalline Materials", p 309 (Coll. Acad. 2021) DOI:10.23647/ca.md20202508

I. Introduction

Fluoride elpasolites belong to the family of A_2BCX_6 elpasolites, where A and B are alkaline ions, C is trivalent metal ion and X is halogen anion. Fluoride elpasolites have attracted particular interest due to several reasons. First of all, that is the perspectives of practical applications. As compared to oxygen-containing crystals they have wider transparency bandgaps in the IR range, and in VIS or UV ranges it can be adjusted easily by complete or partial substitution of C component. The cubic structure and isolated character of CX_6 complexes provide the possibilities to consider them as ideal host lattices for accommodating trivalent cations in perfect octahedral sites of the crystal structure. Some of them can be employed in tandem solar cells [1], applied as optical or optoelectronic materials in photodetectors, detectors, photocatalytic systems, light-emitting diodes [2, 3], optical cooling, lasers [4-6].

Single crystals of fluoride elpasolites may be grown easily by Bridgman technique (some of them have been grown by Czochralski as well) due to their lower melting temperatures as compared to oxide analogues (specifics of their synthesis and growing have been discussed in [7]). Many of them are rather stable under environmental conditions and mechanically durable, that opens a clear perspective for future applications.

The changes of external parameters cause structural phase transitions in these crystals. The temperature phase transitions have been investigated earlier in [7-16] and phase transitions under hydrostatic pressure as well as P–T phase diagrams in [17, 18]; detailed symmetry analysis was proposed in [19]. It should be pointed out that these successions of phase transitions differ considerably from those observed in oxide analogues, that attracts special interest to them. According to symmetry considerations [11, 20, 21], most of these phase transitions may be initially induced by condensation of the F_{1g} soft mode in the cubic phase under cooling. This silent mode corresponds to rotations of CF_6 groups and is inactive both in Raman and IR absorption spectra, but should activate, split and restore below this transition point. Several attempts have been performed to find such restoring modes in optical spectra [11, 21], but in vain. To explain it, other mechanisms of the cubic phase instability have been proposed, like strong anharmonism of CF_6 rotations, cluster model [7], or ordering of these groups under cooling [11, 22, 23], but they disagree with calorimetric data [24].

Raman spectroscopy is a traditional and quite informative method of phase transition investigations. There are two main complementary approaches to investigate structural phase transitions by Raman spectroscopy: search for soft modes in a low-frequency range and higher frequency hard mode spectroscopy [25, 26]. Softening of a low-frequency mode is a bright demonstration of displacive transitions indicating the unique role of this phonon in the critical lattice dynamics, while minor anomalies of hard lattice modes maybe not so impressive but sometimes could be more informative.

So, the main aim of this work is to analyze mechanisms of high-temperature phase instabilities in $Rb_2K\mathit{Re}F_6$ (*Re* is a rare earth ion) crystals by Raman spectroscopy combining both these approaches.

I.1 Structure, symmetry, phase transitions

All crystals of $Rb_2K\mathit{Re}F_6$ compositions crystallize in a cubic space group $Fm\bar{3}m - O_h^6,\ Z = 4$ [7] (Fig. 1a). This structure is formed of KF_6 and $\mathit{Re}F_6$ octahedral groups connected by common F ions in a three-dimensional framework and alternating along the three four-fold axes of the cubic space group. Rb ions are located in (8c) positions that make their vibrations Raman active in contrast to perovskite cubic lattices. It should be pointed that K–F bonds are rather weak and KF_6 octahedra are mostly a figure of imagination, while $\mathit{Re}F_6$ are quite rigid complex ions, and their typical frequencies of internal vibrations are well known and given in many textbooks like [27].

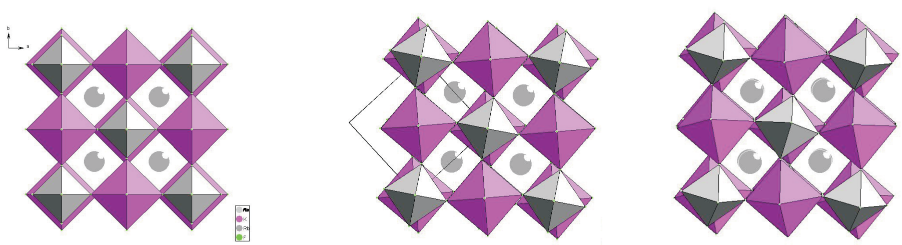

a b c

Figure 1: Structure of $Rb_2K\mathit{Re}F_6$ crystals [22, 23].

a – initial cubic phase, $\Omega(T) = \Omega_0 \exp(-3\gamma_\alpha aT)$**,**

b – tetragonal phase $I114/m - C_{4h}^5,\ Z = 2$**,**

c – monoclinic phase $P12_1/n1 - C_{2h}^5,\ Z = 2$**.**

The cooling results in the first phase transition into the tetragonal phase $P12_1/n1 - C_{2h}^5,\ Z = 2$ [22, 23] (Fig. 1b). This phase transition of the second order does not change volume of the primitive cell so that it can be induced by soft mode condensation at the Brillouin zone center. Further cooling causes the next transition of the first order into monoclinic phase $P12_1/n1 - C_{2h}^5,\ Z = 2$ ², that doubles the primitive cell volume (Fig. 1c). It should be pointed out that transition from the cubic into tetragonal phase is induced by rotations of ReF_6 only, while the next transition is accompanied by both rotations of these groups and displacements of Rb ions. Extensive data about transition temperatures are given in [7, 19].

Greater radii and masses of rare-earth ions move transition temperatures up and narrows tetragonal phase range from 30 K (Re^{3+} = Sc) to 3 K (Re^{3+} = Lu), and for Ho, Y, Tb and Dy this phase disappears completely, so the cubic phase transits into the monoclinic one directly [18] (Fig. 2).

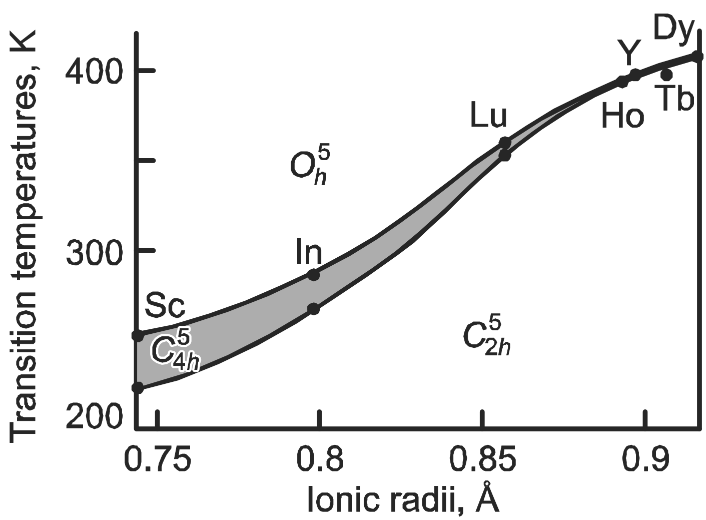

Figure 2: Phase diagram (transition temperarure – Re^{3+} ionic radius) of Rb_2KReF_6 crystals, after [18].

Transition temperatures for the crystals investigated here, according to [22, 28] are given in Table 1.

According to calorimetric measurements, the total entropy change upon transition from the cubic phase to the monoclinic one depends on the size of the trivalent ion as well and increases from 0.7*R* (Sc) to 1.3*R* (Ho). The maximum value (1.3*R*) is quite large for purely displacive transitions but does not allow to assign these transformations to classical order-disorder type [7, 17, 18, 28].

Table 1: Symmetries of distorted phases and transition temperatures for studied crystals

Crystal	Symmetry of distorted phase	Transition temperature, K
Rb_2KScF_6	$I4/m$ $P2_1/n$	252 223
Rb_2KInF_6	$I4/m$ $P2_1/n$	283 264
Rb_2KLuF_6	$I4/m$ $P2_1/n$	370 366
Rb_2KHoF_6	$P2_1/n$	400
Rb_2KDyF_6	$P2_1/n$	390

The vibrational representation of the cubic phase symmetry group in the center of the Brillouin zone is the following:

$$\Gamma_{vib}(Fm\bar{3}m) = A_{1g}(xx, yy, zz) + E_g(xx, yy, zz) + 2F_{2g}(xz,yz,xy) + F_{1g} + 5F_{1u}(x, y, z) + F_{2u}.$$

Given in the brackets are the polarizations of Raman scattering and IR absorption where the corresponding vibrations are active.

Same representations for the tetragonal and monoclinic phases are like these:

$$\Gamma_{vibr}(I114/m) = 3A_g(xx, yy, zz) + 3B_g(xx, yy, xy) + 3E_g(xz, yz) + 5A_u(z) + 6E_u(x, y) + B_u$$

$$\Gamma_{vib}(P12_1/n1) = 12A_g(xx, yy, zz, xy, yx) + 12B_g(xz, yz, zx, zy) + 18A_u(z) + 18B_u(x, y)$$

Tables 2 to 4 show atomic positions in these phases and contributions of ions into the correspoding lattice modes.

Table 2: Symmetry analysis of the cubic phase

Atom	Wyckoff positions	Γ-point phonon modes	
Rb	8c	$F_{2g} + F_{1u}$	
K	4b	F_{1u}	
Re[3+]	4a	F_{1u}	
F	24e	$A_{1g} + E_g + F_{2u} + F_{2g} + 2F_{1u} + F_{1g}$	
Mode classification			
$\Gamma_{Raman} = A_{1g} + E_g + 2F_{2g}$	$\Gamma_{ir} = 4F_{1u}$	$\Gamma_{ac} = F_{1u}$	$\Gamma_{mech} = A_{1g} + E_g + 2F_{2g} + 5F_{1u} + F_{2u} + F_{1g}$

Table 3: Symmetry analysis of the tetragonal phase

Atom	Wyckoff positions	Γ-point phonon modes
Rb	4d	$A_u + B_g + E_g^1 + E_g^2 + E_u^1 + E_u^2$
K	2b	$A_u+E_u^1+E_u^2$
Re[3+]	2a	$A_u+E_u^1+E_u^2$
F(1)	4e	$A_g + E_g^1 + A_u + E_g^2 + E_u^1 + E_u^2$
F(2)	8h	$2A_g + 2B_g + E_g^1 + E_g^2 + 2E_u^1 + 2E_u^2 + A_u + B_u$
Mode classification		
$\Gamma_{Raman} = 3A_g + 3B_g + 3E_g^1 + 3E_g^2$	$\Gamma_{ir} = 4A_u + 5E_u^1 + 5E_u^2$ $\Gamma_{ac} = A_u + E_u$	$\Gamma_{mech} = 3A_g + 3B_g + 3E_g^1 + 3E_g^2 + 5A_u + 6E_u^1 + 6E_u^2 + B_u$

Table 4: Symmetry analysis of the monoclinic phase

Atom	Wyckoff position	Γ-point phonon modes
Rb	4e	$3E_g + 3B_g + 3A_u + 3B_u$
K	2c	$3A_u + 3B_u$
Re^{3+}	2a	$3A_u + 3B_u$
F(1)	4e	$3E_g + 3B_g + 3A_u + 3B_u$
F(2)	4e	$3E_g + 3B_g + 3A_u + 3B_u$
F(3)	4e	$3E_g + 3B_g + 3A_u + 3B_u$
	Modes classification	
$\Gamma_{Raman} = 12A_g + 12B_g$	$\Gamma_{ir} = 17A_u + 16B_u$ $\Gamma_{ac} = A_u + 2B_u$	$\Gamma_{mech} = 12A_g + 12B_g + 18A_u + 18B_u$

We can expect the appearance of new lines below transition points due to symmetry lowering, splitting of degenerate modes and cell doubling in the monoclinic phases. It should be pointed out that potassium and rare earth ions stay at the centers of symmetry in all phases and their vibrations are Raman inactive.

II. Experiment

The crystals of the elpasolites were synthesized in a solid-phase chemical reaction from a mixture of the fluorides RbF, KF, and ReF_3 taken in the appropriate proportions. The precursors taken in stoichiometric amounts were melted in the sealed platinum ampules in an argon atmosphere. After slow cooling, the boules with transparent inclusions were obtained. The single crystals were grown from selected transparent parts of the boules by Bridgeman–Stockbarger method. Samples for experiments were optically transparent [6] and without defects or inclusions visible under the microscope, with a diameter of 9–10 mm and 5–10 mm length.

Raman scattering spectra of crystals under investigations have been studied in a temperature range from 7 K to 600 K. Spectra were collected in backscattering geometry, using a triple monochromator Jobin Yvon T64000 Raman spectrometer operating in subtractive mode, then detected by a CCD cooled at 140 K. The spectral resolution for the recorded Stokes side Raman spectra was set to 1 cm^{-1} (this resolution was achieved using 1800 grooves/mm gratings and 100 μm slits). The microscope system based on Olympus BX41 microscope with a 50× objective lens *f* = 10.6 mm of NA 0.5 provides a focal spot diameter of about 5 μm on the sample. Single-mode argon 514.5 nm of Spectra-Physics Stabilite 2017 Ar^+ laser of 100 mW power (15 mW on the sample) was used as excitation light source.

Additionally, IR absorption spectra were recorded from Rb_2KLuF_6 crystal in a temperature range from 273 K to 463 K in polyethylene matrix using a Vertex 70 (Bruker) spectrometer in the range 70–650 cm^{-1} with resolution 1 cm^{-1}. The temperature measurements were made with the same Specac cryostat.

III. Experimental results

Typical polarized Raman spectra of Rb_2KScF_6 crystal are shown in Fig. 3.

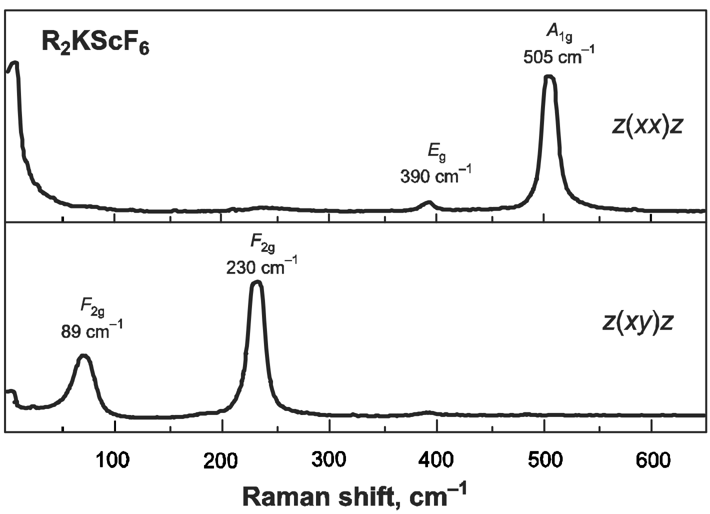

Figure 3: Polarized Raman spectra of Rb_2KScF_6 crystal in the cubic phase (room temperature). The sample was oriented along cubic unit cell axes.

All lines are well polarized and rather narrow, confirming perfectly ordered cubic structure of the crystal. Three higher frequency Raman lines correspond to internal modes of ScF_6 octahedra while the lower frequency line should represent lattice vibrations of Rb ions. Spectra of all other studied crystals in their cubic phases look very much the same; line positions and eigenvectors of lattice modes are shown in Table 5 according to [27].

Table 4: Eigenvectors, symmetries and band positions (cm^{-1})
of observed spectral lines
in the cubic phase of the $Rb_2K\mathit{Re}^{3+}F_6$ crystals

Eigenvector	Irreducible representation	Rb_2KLuF_6 this work	Rb_2KHoF_6 [8]	Rb_2KDyF_6 [8]	Rb_2KScF_6 [9]	Rb_2KInF_6 [10]	Rb_2KYF_6 [11]
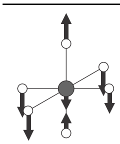	F_{1u} (IR)	390					
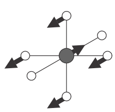	F_{1u} (IR)	178 (LO) 149 (TO)					
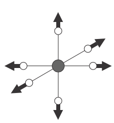	A_{1g} (Raman)	484	472	470	505	507	470
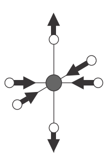	E_g (Raman)			380	390	379	
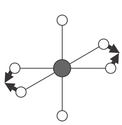	F_{2g} (Raman)	210	204	202	230	218	210
Rb	F_{2g} (Raman)	62	61	65	89	69	60

Transformations of higher and lower parts of this spectrum are shown in Fig. 4.

Cooling results in a slight gradual shift down and narrowing of the totally symmetrical internal mode, as well as the appearance of a weak new line due to cell doubling in the monoclinic phase. In the lower frequency part, a lot of new lines emerge below phase transitions, shifting up under further cooling. Temperature dependence of the lowest lines positions is shown in Fig. 5.

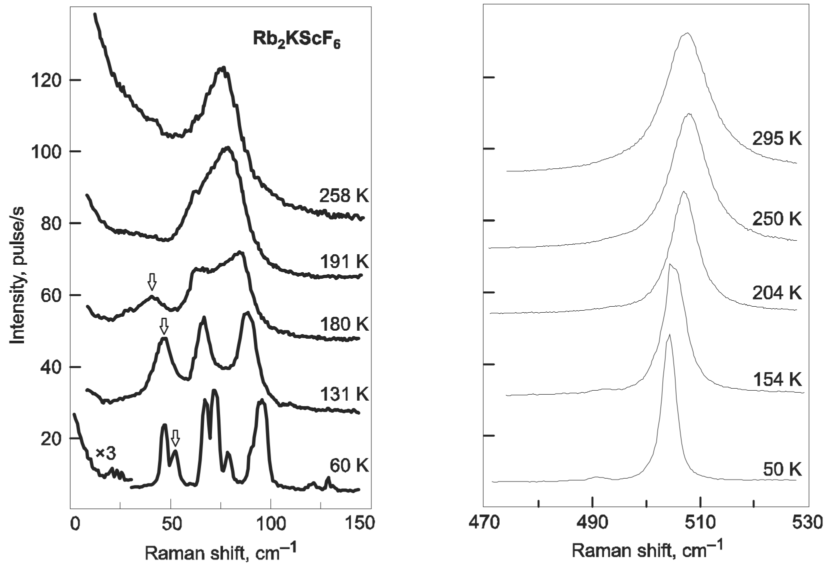

Figure 4: Transformations of lower and higher frequency parts of Raman spectra of Rb_2KScF_6 crystal.

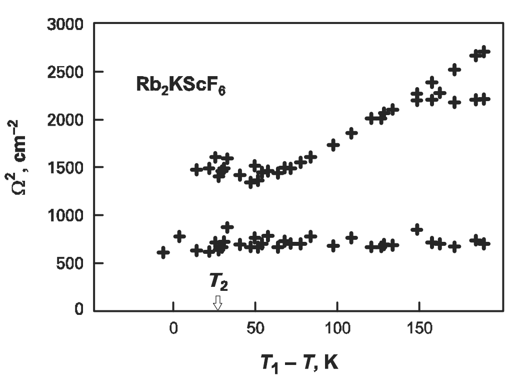

Figure 5. Squared frequencies of the lowest Raman lines vs temperature in Rb_2KScF_6 crystal.

There is a line with squared frequency growing linearly under cooling below the transition point, that is typical for a soft mode behavior, but there exists one more mode with a lower frequency that does not change at all.

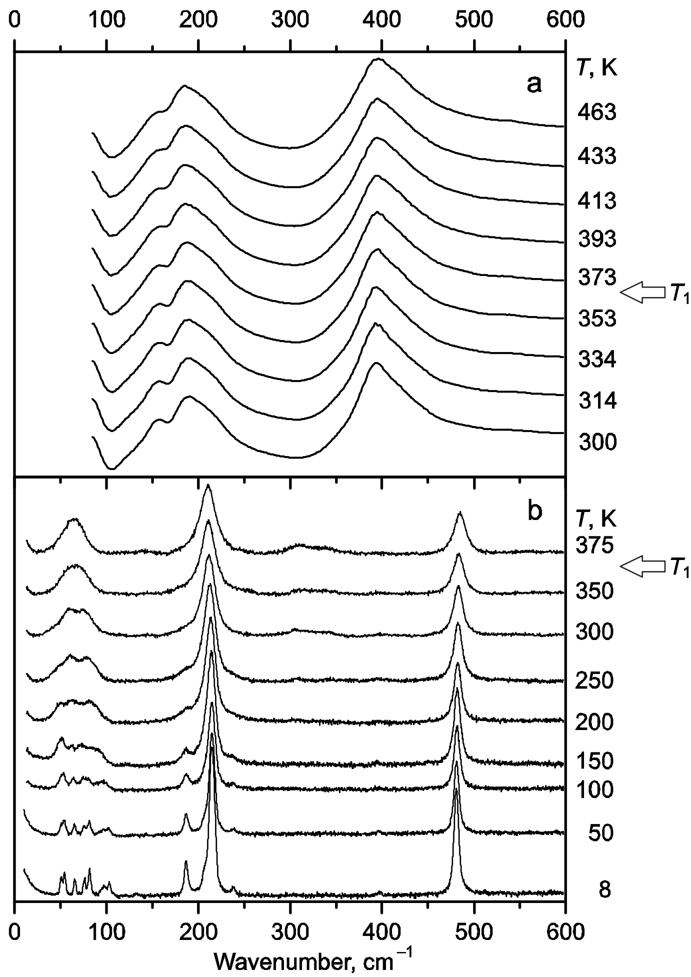

Figure 6: Transformation of Rb_2KLuF_6 spectra vs temperature.
a – infrared absorption, b – Raman scattering.

Fig. 6 demonstrates temperature transformations of Raman and IR absorption spectra, obtained with powder samples of Rb_2KLuF_6.

IV. Discussion

To discuss obtained results quantitatively all obtained spectra have been numerically treated. Spectral parameters of Raman lines have been obtained using damped harmonic oscillator functions.

IV.1 Low-frequency lattice modes

As it was shown above (see Fig. 5), no typical soft mode behavior restoring below transition points was found, in agreement with previous data [7, 11]. According to symmetry analysis, such modes should correspond to rotations of ReF$_6$ groups. Lattice dynamics of the monoclinic phase of these crystals have been simulated within both empirical and first principal approaches [21]. Frequencies of the cubic and tetragonal lattices (simulated at zero kelvins) are shown in Table 5 with experimental results. Naturally enough structures of the cubic and tetragonal phases are unstable below corresponding transition points that results in appearence of several imaginary frequencies in simulated spectra. These low-frequency F_{1g} and F_{2g} unstable modes could give rise to the soft mode restorations in the tetragonal and monoclinic phases.

Table 5: The simulated and experimental Raman frequencies of Rb_2KScF_6 crystal in the cubic and tetragonal phases.

*Fm*3*m*	Ω_{cal}, cm^{-1}	Ω_{exp}, cm^{-1}	*I*4/*m*	Ω_{cal}, cm^{-1}	Ω_{exp}, cm^{-1}
F_{1g}	66*i*		E_g	54*i*	26
			A_g	20	39
F_{2g}	26*i*	89	B_g	18	84
			E_g	23	91
F_{2g}	152	230	E_g	152	230
			B_g	152	233
E_g	343	390	A_g	325	392
			B_g	336	
A_{1g}	402	505	A_g	385	506

Simulated frequencies of these modes agree reasonably with experimental results while obtained eigenvectors include considerable components of cations displacements (Table 6). There are no modes connected with octahedra rotations exclusively – obviously, such rotations strongly interact with cation displacements in the monoclinic phase.

Such interactions of rotational and displacive degrees of freedom are symmetry forbidden in higher symmetry phases but become permitted in the low symmetry monoclinic structure, as it was noted in [22].

Replacing scandium for heavier rare-earth ions moves these noncritical low-frequency lattice modes down, increases this interaction and as a result, destroys the cubic phase at higher temperatures [8].

Table 6: Eigenvectors for lowest lattice modes of the monoclinic phase in Rb_2KScF_6 (only nonzero components are shown).

		Rb	Rb	Rb	Rb	F	F	F	F	F	F	F	F	F	F	F	F
	x	–0.1	0.1	0.1	0.1	0.0	–0.1	0.1	0.0	–0.1	0.1	0.0	0.1	–0.1	0.0	0.1	–0.1
22 cm^{-1}	*y*	0.3	0.3	0.2	–0.2	0.1	–0.1	0.1	–0.1	0.1	–0.1	0.1	–0.1	0.1	–0.1	0.1	–0.1
	z	0.3	0.3	0.4	–0.4	0.0	–0.1	–0.1	0.0	–0.1	–0.1	0.0	0.1	0.1	0.0	0.1	0.1
	x	0.0	0.0	0.1	–0.1	0.0	–0.1	0.0	0.0	0.1	–0.1	0.0	0.0	0.0	0.0	0.0	–0.1
29 cm^{-1}	*y*	–0.4	–0.3	0.6	0.4	0.1	–0.1	0.0	0.1	–0.1	0.0	–0.1	0.0	–0.1	–0.2	0.0	–0.1
	z	0.0	0.0	–0.1	0.0	0.0	0.1	0.0	0.0	0.0	0.1	0.0	0.1	0.0	0.0	0.0	0.1
	x	0.4	0.4	–0.4	–0.4	0.0	–0.1	–0.1	0.0	–0.1	–0.1	0.0	0.1	0.1	0.0	0.1	0.1
31 cm^{-1}	*y*	–0.1	0.1	–0.1	0.1	0.0	–0.1	–0.1	0.0	0.1	0.1	0.0	–0.1	–0.1	0.0	0.1	0.1
	z	0.1	0.1	–0.1	–0.1	0.0	–0.2	0.1	0.0	–0.2	0.1	0.0	0.2	–0.1	0.0	0.2	–0.1
	x	–0.1	–0.1	0.2	0.1	0.0	0.0	0.1	0.0	0.0	0.1	0.0	0.0	–0.1	0.0	0.0	–0.1
37 cm^{-1}	*y*	–0.4	0.4	–0.4	0.4	–0.1	0.0	0.1	0.1	0.0	–0.1	–0.1	0.0	0.1	0.1	0.0	–0.1
	z	0.2	0.2	–0.2	–0.2	0.0	0.0	0.0	0.0	0.0	0.0	0.0	0.0	0.0	0.0	0.0	0.0
	x	–0.4	0.4	–0.5	0.5	–0.1	0.0	0.0	0.1	0.0	0.0	0.0	0.0	0.0	0.0	0.0	0.0
43 cm^{-1}	*y*	0.0	0.0	0.0	0.1	0.0	0.0	0.0	0.0	0.0	0.0	–0.1	0.0	0.0	0.0	0.0	0.0
	z	0.0	0.1	0.1	–0.1	0.0	0.0	0.0	0.0	0.0	0.0	0.0	0.0	0.0	–0.1	0.0	0.0

IV.2 High-frequency internal modes

Temperature transformation of the highest frequency internal mode of ScF_6 group has been shown in Fig. 4. Positions of these modes for Sc and In crystals vs temperature are given in Fig. 7.

Curves at these graphs correspond to extrapolations of these dependencies in the cubic phases with following equation:

$$Fm\overline{3}m - O_h^6, Z = 4$$

where Ω_0 is the frequency at zero temperature, γ_α – Gruneisen parameter, *a* – temperature expansion, $\Omega_0 = 518$ cm^{-1}, $\gamma_\alpha a = 0.2 \cdot 10^{-5}$ K^{-1} for Rb_2KScF_6 and $\Omega_0 = 514$ cm^{-1}, $\gamma_\alpha a = 1.5 \cdot 10^{-4}$ K^{-1} for Rb_2KInF_6.

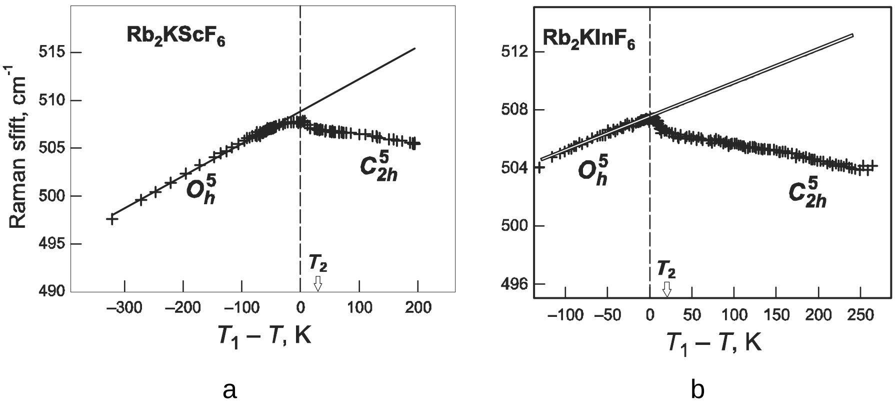

Figure 7: Temperature dependences of the highest frequency internal mode for Rb_2KScF_6 (a) and Rb_2KInF_6 (b) crystals.

A linear deviation of these frequencies from the extrapolated values is seen, that is supposed to be proportional to the order parameter below phase transitions of the second order or the first order close to the tricritical point.

Temperature dependence of this line width in Rb_2KScF_6 crystal is shown in Fig. 8.

The curve in the figure is the extrapolation of this dependence in the cubic phase with the equation:

$$\sigma(\Omega_\alpha,\ T) = \sigma(\Omega_\alpha,\ 0)\left(1 + \frac{1}{\exp(\hbar\Omega_{\beta 1} / k_B T) - 1} + \frac{1}{\exp(\hbar\Omega_{\beta 2} / k_B T) - 1}\right)$$

that corresponds to the phonon Ω_α decay into $\Omega_{\beta 1}$ (410 cm^{-1}) and $\Omega_{\beta 2}$ (100 cm^{-1}) due to the anharmonicity of lattice dynamics.

A perfect agreement of experimental data with this dependence is seen, and no feature of Arrenius dependence typical for ordering processes was found. Slight change of this dependence below the phase transition is induced obviously by alterations of lower frequency lattice dynamics.

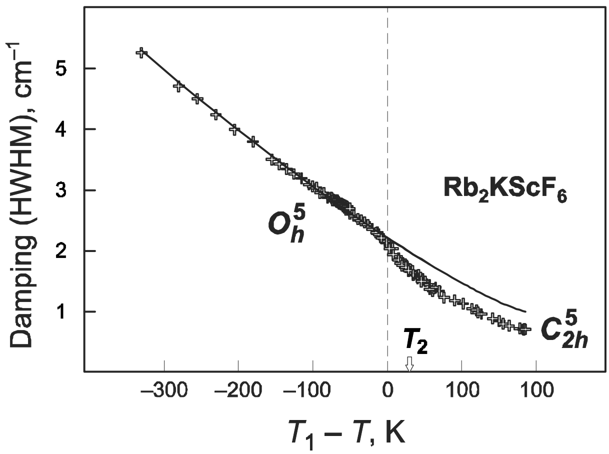

Figure 8: Temperature dependence of the damping constant (half width at half maximum) for the highest line in Rb_2KScF_6 spectrum.

V. Conclusion

Phase transitions in the studied crystals are induced by condensation of soft phonon modes, corresponding to rotations of ReF_6 groups. No signs of order-disorder processes were found. The temperature dependence of hard mode frequencies shows that the behavior of the order parameter is typical for phase transitions of the second type, or the first type close to the tricritical point. In the low-frequency region, the strong interaction of order parameter fluctuations with noncritical lattice vibrations (fluctuations of secondary order parameters) is observed, that explains the absence of restoring soft modes in Raman spectra below the phase transitions. Increasing the mass of a rare-earth ions shifts dynamics of noncritical modes to the lower-frequency region, that enhances this interaction and leads to a narrowing of the range of existence of the tetragonal phase and then to its disappearance.

Acknowledgement:

A. Vtyurin, A. Krylov, S. Krylova, Yu. Gerasimova, A. Ivanenko, V. Voronov

This work was partly supported by the Russian Foundation for Basic Research Grant no 18-02-00754.

Complementary informations on authors:

vtyurin@iph.krasn.ru, ORCID 0000-0002-8816-4995

shusy@iph.krasn.ru, ORCID 0000-0001-8949-0584

slanky@iph.krasn.ru, ORCID 0000-0003-1277-6044

Cite this paper: A. Vtyurin, A. Krylov, S. Krylova, Yu. Gerasimova, A. Ivanenko, V. Voronov, OAJ materials and Devices, vol 5(1) – chap No9 in “Perovskites and other Framework Structure Crystalline Materials”, p 309 (Coll. Acad. 2021) DOI:10.23647/ca.md20202508

REFERENCES

1. E. Meyer, D. Mutukwa, N. Zingwe and R. *Taziwa Lead-Free Halide Double Perovskites: A Review of the Structural, Optical, and Stability Properties as Well as Their Viability to Replace Lead Halide Perovskites*, *Metals* 8, p 667 (2018).
2. L. Chu, W. Ahmad, W. Liu et al. *Lead-Free Halide Double Perovskite Materials: A New Superstar Toward Green and Stable Optoelectronic Applications*, in *Nano-Micro Lett.* 11:16 (2019).
3. H. Wei, M. Du, L. Stand, Z. Zhao, H. Shi, M. Zhuravleva, and C.L. Melcher *Scintillation Properties and Electronic Structures of the Intrinsic and Extrinsic Mixed Elpasolites* $Cs_2NaRBr_3I_3$ *R* = (La, Y), *Phys. Rev. Applied* 5, 024008 (2016).
4. S. R. Bowman, C. E. Mungan, *New materials for optical cooling*, *Appl. Phys. B* 71, p 807 (2000).
5. P. A. Tanner, *Spectra, energy levels and energy transfer in high symmetry lanthanide compounds, Top. Curr. Chem*. 241, p 167 (2004).
6. B. F. Aull, H. P. Jenssen*, Impact of ion-host interactions on the 5d-to-4f spectra of lanthanide rare-earth-metal ions. II. The Ce-doped elpasolites, Phys. Rev. B* 34, p 6647 (1986).
7. I. N. Flerov, M. V. Gorev, K. S. Aleksandrov, A. Tressaud, J. Grannec, and M. Cousi, *Phase transitions in elpasolites (ordered perovskites). Mater. Sci. Eng. R* 24, p 81 (1998).

8. A. Vtyurin, A. Krylov, V. Voronov, S. Krylova *Raman scattering and phase transitions in fluorides with elpasolite structure, in Ferroelectrics* 512, p 58 (2017).

9. S. N. Krylova, A. N. Vtyurin, A. Bulou, A. S. Krylov, N.G. Zamkova *Lattice dynamics and Raman scattering spectrum of elpasolite Rb_2KScF_6: Comparative analysis, Phys. Solid State*. 46, is 7, p 1311 (2004).

10. A. S. Krylov, S. N. Krylova, A. N. Vtyurin, V. N. Voronov, A. S. Oreshonkov *Raman Scattering Study Temperature Phase Transitions of Rb_2KInF_6 Crystal*, *Ferroelectrics*, 416, p 95 (2011).

11. M. Couzi, S. Khaïroun, A. Tressaud A. *Structural Phase Transitions in $Rb_2KM^{III}F_6$ Elpasolites. II. Raman scattering and group theoretical studies of Rb_2KFeF_6 and Rb_2KYF_6*, *Physica status solidi (a)* 98, is 2, p 423 *(1986).*

12. B. V. Beznosikov, I. M. Flerov, M. V. Gorev, S. V. Melnikova, S. V. Misjul, V. N. Voronov *Structural phase transitions in elpasolites Rb_2NaDyF_6 and Rb_2KDyF_6, Ferroelectrics Letters Section*, 1, p 35–41 (1983).

13. I. N. Flerov, M. V. Gorev, V. N. Voronov, A. Tressaud, J. Grannec, H. Guengard *Thermodynamic properties of elpasolites $Rb_2KB^3F_6$ (B^3: Er, Ho), Ferroelectrics*, 168, 1, p 55-60, (1995).

14. A. S. Krylov, A. N. Vtyurin, A. S. Oreshonkov, V. N. Voronov and S. N. Krylova *Structural transformations in a single-crystal Rb_2NaYF_6: Raman scattering study. J. Raman Spectrosc.*, 44, p 763–769, (2013).

15. A. Krylov, A. Vtyurin, V. Voronov, S. Krylova *Manifestations of Structural Phase Transitions in a Rb_2KLuF_6 Crystal in Its Raman Spectra, Optics and Spectroscopy* 126, is 4, p 423–427 (2019).

16. A. S. Krylov, A. N. Vtyurin, V.N. Voronov and S. N. Krylova *Phase transitions in Rb_2KLuF_6 crystal, Ferroelectrics* 538, p 28–34 (2019).

17. M. V. Gorev, I. N. Flerov, V. N. Voronov, S. V. Misyul' *Pressure-temperature phase diagrams of elpasolites $Rb_2KB^{3+}F_6$ (B^{3+} =Ho, Dy, Tb). Phys. Solid State*, 35, Is 4, p 524-527 (1993).

18. I. N. Flerov, M. V. Gorev, S. V. Melnikova, S. V. Misyul, V. N. Voronov, K. S. Aleksandrov *Phase transitions in elpasolite Rb_2KScF_6. Phys. Solid State*, 34, 2185 (1992).

19. K. S. Aleksandov and J. Bartolome, *Structural distortions in families of perovskite-like crystals. Phase Transitions*, 74, p 255 (2001).

20. P.Selgert, C.Lingner, B.Luthi *On the structural phase transition in rare earth elpasolites. Z. Phys. B – Cond. Matt.*, 55, p 219 (1984).

21. A.S. Krylov, A. Bulou, S.N. Krylova. *Symmetry analysis of calculated vibrational spectra of Rb_2KScF_6 crystal, Computational Materials Science* 36, Is 1-2, p 221-224 (2006).

22. I. N. Safonov, S. V. Misyul, M. S. Molokeev, M. P. Ivliev *Structural transformations and phenomenological description of the formation of phase tsates in elpasolites Cs_2RbDyF_6 and $Rb_2KB'F_6$ (B' = Ho, Dy, Tb). Phys. Solid State*, 57, p 491 (2015).

23. K. S. Aleksandrov, S. V. Misyul, M. S. Molokeev, V. N. Voronov*, Structures of distorted phases and critical and noncritical atomic displacements of elpasolite Rb_2KInF_6 during*

phase transitions, Phys. Solid State, 51, p 2505, (2009).

24. I. N. Flerov, M. V. Gorev, K. S. Aleksandrov, A. Tressaud, V. D. Fokina *Ferroelastic phase transitions in fluorides with cryolite and elpasolite structures*. *Crystallography Reports*, 49, p 100-107, (2004).
25. E. K. H. Salje *Hard mode spectroscopy: experimental studies of structural phase transitions, Phase Transitions,* 37, p 83-110 (1992).
26. U. Bismayer *Hard mode Raman spectroscopy and its application to ferroelastic and ferroelectric phase transitions, Phase Transitions*, 27, p 211-267 (1990).
27. K. Nakamoto, *Infrared and Raman Spectra of Inorganic and Coordination Compounds* Wiley, New York (1986).
28. I. N. Flerov and M. V. Gorev. *Entropy and the Mechanism of Phase Transitions in Elpasolites. Phys. Solid State*, 43, p 127–136 (2001).